# Analysis of an Extremum Seeking Controller Under Bounded Disturbance

Samuel C. Pinto[1] and Sean B. Andersson[1,2]
[1]Department of Mechanical Engineering, [2]Division of Systems Engineering,
{samcerq,sanderss}@bu.edu

***Abstract*— One of the applications of Extremum Seeking (ES) is to localize the source of a scalar field by using a mobile agent that can measure this field at its current location. While the scientific literature has presented many approaches to this problem, a formal analysis of the behavior of ES controllers for source seeking in the presence of disturbances is still lacking. This paper aims to fill this gap by analyzing a specific version of an ES control algorithm in the presence of source movement and measurement disturbances. We define an approximate version of this controller that captures the main features but allows for a simplified analysis and then formally characterize the convergence properties of this approximation. Through simulations and physical experiments, we compare the theoretically-predicted regions of attraction of the simplified system with the behavior of the full system and show that the simplified version is a good predictor of the behavior of the initial ES controller.**

## I. INTRODUCTION

In this paper we consider the problem of tracking a moving source using a mobile agent. We consider that the agent senses this moving source using scalar measurements, and that these measurements are stronger the closer the agent is to the source. This paradigm can be used to model a wide variety of practical engineering scenarios, such as particle tracking using a confocal microscope [1], [2], localizing acoustic sources using drones [3] and tracking moving targets using WiFi-based radars [4]. A common approach to these types of problems is that of Extremum Seeking (ES) (see [5] for a review of the field). More recently, approaches such as optimization based schemes for ES [6] and heuristic-based circular motions with proven stability [7], [8] have been of particular interest for source seeking.

In previous works from our group [1], [2], we built upon the results in [8] to create a source-seeking ES controller. In this formulation, the controller seeks to converge to a circular movement around the source with a radius defined as a controller parameter. Note that in applications where the goal is to estimate the position of a (fixed) source in a two-dimensional setting, the optimal policy in terms of the corresponding Cramer-Rao lower bound on the estimate of the position is to move in a circle around the source with a radius that depends on the observation model parameters [1]. This approach is appealing because a circular motion with constant linear velocity tends to be easy to implement in real world systems, particularly for systems with non-holonomic kinematics. The control law is also computationally simple and is based only on the local measurement, independent of any global knowledge, making it useful for systems with fast dynamics and limited computational power.

The global convergence of this ES controller was proven for a static source in [8]. However, simulations [1] and physical experiments [9] have shown that this convergence is *not* global in practical scenarios. In this paper, our main goal is to explain this discrepancy between the existing theory and the practical application, as well as to provide a formal and systematic way to design the system parameters, with predictable and well-characterized regions of attraction. In order to achieve this goal, instead of using the exact ES formulation in [8], we consider an approximate version with a simpler algebraic formulation that still captures the salient features of the original controller. By using this approximate version, we show that in the presence of disturbances in the measurement and the movement, the controller is guaranteed to steer the agent towards an approximately circular orbit around the source if its initial location is within a certain distance from the source. Then, we use simulations to demonstrate that the behavior of the simplified controller is indeed similar to the original one and that the predictions on the convergence region based on the simplified controller are a good predictor of the behavior of the initial ES controller. We note that this simplified version of the controller is intended only as a tool for analysis, not as a practical controller.

## II. EXTREMUM SEEKING CONTROLLER

In the source seeking problem, we consider an agent trying to find a source in a two dimensional environment. This source is able to move, though its movement model is unknown to the agent. In order to simplify future calculations, we assume that the reference frame is always centered on the source, and thus its location is $\begin{bmatrix}0 & 0\end{bmatrix}^T$. The dynamics of the position of the agent, $s(\cdot)$, is given by

$$\dot{s}(t) = u(t) - w(t), \tag{1}$$

where $u(t)$is the control input and $w(t)$ is an unknown disturbance that accounts for the source movement. We assume that $w(t)$ is bounded, with $||w(t)|| < M_w$ where $||\cdot||$ is the usual $\mathcal{L}_2$ norm.

This work was supported in part by NSF under grant ECCS-1931600 and by the NIH under grant 1R01GM117039-01A1.

For many real-world scalar signals of interest (such as the fluorescence intensity of a single fluorescent particle in a confocal microscope, or the measured power of an electromagnetic wave), the signal decays smoothly as a function of distance, reaching zero only when that distance tends to infinity. Of course, in practice, any such measurement is corrupted by measurement noise. To capture this, we assume the agent can continuously acquire a signal $y(\cdot)$ of the scalar field $f(\cdot)$ according to the measurement model

$$y(t) = f(||s(t)||) + v(t), \tag{2}$$

where $v(t)$ is a bounded disturbance, with $||v(t)|| < M_v$ and $f : \mathbb{R}^+ \to \mathbb{R}^+$. We assume the function $f(\cdot)$ satisfies the following technical assumptions to ensure smoothness:

1) $f(\cdot)$ is differentiable and its derivative is bounded;
2) $f(\cdot)$ is strictly decreasing;
3) $f(\xi) > 0$ for all $\xi \in \mathbb{R}^+$;
4) $\lim_{\xi\to\infty} f(\xi) = 0$;

Note that these are generally satisfied by most real-world signals of interest and are thus not particularly restrictive.

To move towards the source location, we use the ES controller introduced in [8] and refer to it as the Original ES Controller (OESC). The OESC is given by

$$u(t) = \begin{bmatrix} -\omega R \sin(\theta(t)) \\ \omega R \cos(\theta(t)) \end{bmatrix}, \tag{3a}$$

$$\dot{\theta}(t) = \omega - k_p \frac{d}{dt}\left(y(s(t), v(t))\right), \tag{3b}$$

where $R$, $\omega$ and $k_p$ are positive constants chosen by the designer and can be understood as a radius, angular velocity and proportional controller gain, respectively.

In order to give some intuition on the behavior of this controller, we highlight that in the absence of sensing disturbance or source movement (i.e. $w = v = 0$), the OESC steers the system to a limit cycle given by a circular orbit with radius $R$ around the source. Note that the control law only adjusts the angular velocity $\dot{\theta}$ to steer the system to this orbit. Global convergence to this limit cycle (in the absence of disturbances) was shown in [8]. This controller has many interesting practical features, such as the fact that its linear velocity is constant and that it is inherently able to handle non-holonomic kinematics. Moreover, simulations and experiments with real hardware, as will be discussed later in this paper, show that the trajectories generated using this controller are smooth and easily followed by physical systems such as mobile robots.

**Simplified Extremum Seeking Controller:** The main goal of this paper is to study the behavior of the OESC in the presence of source movement and disturbances in the measurements. To achieve this, we now develop a simplified version of the OESC, denoted the Simplified ES Controller (SESC), that captures the main features of the behavior but is more amenable to analysis.

To this end, consider first the OESC with $w = v = 0$. We define the instantaneous center of the motion, $c(t)$, as

$$c(t) = s(t) - R \begin{bmatrix} \cos(\theta(t)) \\ \sin(\theta(t)) \end{bmatrix}, \tag{4}$$

where $R = v/\omega$. The time derivative of $||c(t)||$ is

$$\frac{d}{dt}||c(t)|| = \frac{c^T(t)\dot{c}(t)}{||c(t)||}. \tag{5}$$

Using (3) in this expression yields

$$\frac{d}{dt}||c(t)|| = -k_p \omega R \frac{dy(t)}{dt} \frac{c^T(t)}{||c(t)||} \begin{bmatrix} -\sin(\theta(t)) \\ \cos(\theta(t)) \end{bmatrix}. \tag{6}$$

Note that $c(t)/||c(t)||$ is a unit vector that gives the direction to the instantaneous center from the origin (that is, from the source location). We denote this unit vector as

$$c(t)/||c(t)|| = \begin{bmatrix} \cos(\alpha(t)) & \sin(\alpha(t)) \end{bmatrix}^T. \tag{7}$$

From this we can rewrite (6)

$$\frac{d}{dt}||c(t)|| = k_p \omega R \frac{dy(t)}{dt} \sin\left(\theta(t) - \alpha(t)\right). \tag{8}$$

This shows that the behavior of the OESC is to drive the agent along a circular path of radius $R$ around the center $c(t)$ while simultaneously continuously moving that center towards the origin according to (8).

The difficulty in analyzing the OESC is at least in part due to the continuous motion of the center of the rotation. Therefore, in the SESC, our goal is to maintain the same average feedback of the OESC, but to make the center of rotation fixed for a full rotation before updating. Then, the dynamics of the agent are as in (3), but with the angle dynamics $\dot{\theta}(s)$ replaced by:

$$\dot{\theta}(t) = \omega,\ t \in (t_0[k], t_0[k] + T), \tag{9}$$

where $T = \frac{2\pi}{\omega}$ and $t_0[k]$ is the the beginning of the $k$-th revolution. The center of rotation $c[k]$is instantaneously translated at the end of each revolution according to

$$c[k+1] = c[k] + k_p \gamma[k], \tag{10}$$

where $\gamma[k]$ is given by

$$\gamma[k] = \int_0^T y(t + t_0[k]) \begin{bmatrix} \cos(\omega t + \theta(t_0[k])) \\ \sin(\omega t + \theta(t_0[k])) \end{bmatrix} dt. \tag{11}$$

Intuitively, the SESC computes $\gamma$ by doing an average of the signal received during its circular motion, "weighted" by the direction. The closer the agent is to the source, the higher the intensity of the signal is. It is thus expected that, in the absence of noise, $\gamma$ will point towards the source. We will show below that the norm of $\gamma$ is equivalent to the average OESC feedback effect on the rotation center, given by (8).

We now show that the feedback of the SESC is analogous to the OESC in terms of the revolution center displacement. If the agent movement is perfectly circular, then its velocity is given by

$$\dot{s} = \begin{bmatrix} -v \sin(\omega t) \\ v \cos(\omega t) \end{bmatrix}. \tag{12}$$

Given this movement policy for the agent, we can integrate (8) over one period. Integrating by parts, we get:

$$\int_{t_0}^{t_0+T} \frac{dy(t)}{dt} \sin(\omega t - \alpha) dt = \frac{1}{\omega} \int_0^T y(t+t_0) \cos(\omega t + \theta(t_0) - \alpha) dt. \quad (13)$$

Prop. 1 below shows that the integral in (13) (which represents the average feedback effect of the OESC) is equivalent to $||\gamma||$. Moreover, we show that the equivalent feedback $\gamma$ is directed towards the source.

*Proposition 1:* Under the agent policy in (12), we have

$$\|\gamma\| = \left\| \int_0^T y(t+t_0) \cos(\omega t + \theta(t_0) - \alpha) dt \right\|, \quad (14a)$$

$$\frac{\gamma}{\|\gamma\|} = -\frac{c}{\|c\|}. \quad (14b)$$

Additionally, $||\gamma||$ only depends on $||c||$.

*Proof:* First note that

$$y(t+t_0) = y\left( \left\| c + R \begin{bmatrix} \cos(\omega t + \theta(t_0)) \\ \sin(\omega t + \theta(t_0)) \end{bmatrix} \right\| \right). \quad (15)$$

Introducing the change of variables $t' = t - (\theta_0(t_0) - \alpha)/\omega$ into (11) yields

$$\gamma = \int_0^T y\left( \left\| c + R \begin{bmatrix} \cos(\omega t - \alpha) \\ \sin(\omega t - \alpha) \end{bmatrix} \right\| \right) \begin{bmatrix} \cos(\omega t - \alpha) \\ \sin(\omega t - \alpha) \end{bmatrix} dt. \quad (16)$$

Note that

$$\begin{bmatrix} \cos(\omega t - \alpha) \\ \sin(\omega t - \alpha) \end{bmatrix} = \underbrace{\begin{bmatrix} \cos(\alpha) & \sin(\alpha) \\ -\sin(\alpha) & \cos(\alpha) \end{bmatrix}}_{\mathcal{U}} \begin{bmatrix} \cos(\omega t) \\ \sin(\omega t) \end{bmatrix}. \quad (17)$$

Thus, $\gamma$ is given by

$$\mathcal{U} \int_0^T y\left( \left\| \mathcal{U} \left( \begin{bmatrix} ||c|| \\ 0 \end{bmatrix} + R \begin{bmatrix} \cos(\omega t) \\ \sin(\omega t) \end{bmatrix} \right) \right\| \right) \begin{bmatrix} \cos(\omega t) \\ \sin(\omega t) \end{bmatrix} dt. \quad (18)$$

Since $\mathcal{U}$ is a rotation matrix, it does not affect the norm of the vector. Therefore, we have

$$\gamma = \mathcal{U} \int_0^T y\left( \left\| \begin{bmatrix} ||c|| \\ 0 \end{bmatrix} + R \begin{bmatrix} \cos(\omega t) \\ \sin(\omega t) \end{bmatrix} \right\| \right) \begin{bmatrix} \cos(\omega t) \\ \sin(\omega t) \end{bmatrix} dt. \quad (19)$$

Thus (19) shows that $||\gamma||$ only depends on $||c||$. Then,

$$\left\| \begin{bmatrix} ||c|| \\ 0 \end{bmatrix} + R \begin{bmatrix} \cos(\omega t) \\ \sin(\omega t) \end{bmatrix} \right\| = \underbrace{\sqrt{||c||^2 + R^2 + 2\|c\| R \cos(\omega t)}}_{g(t)} \quad (20)$$

Consequently, (19) can be rewritten as

$$\int_0^T y(g(t)) \begin{bmatrix} \cos(\omega t) \\ \sin(\omega t) \end{bmatrix} dt = \int_0^{\frac{T}{2}} y(g(t)) \begin{bmatrix} \cos(\omega t) \\ \sin(\omega t) \end{bmatrix} dt + \int_{\frac{T}{2}}^T y(g(t)) \begin{bmatrix} \cos(\omega t) \\ \sin(\omega t) \end{bmatrix} dt \quad (21)$$

Then we introduce the change of variables $t' = T - t$ in the second part of the integral and use the fact that $\sin(\omega t) = -\sin(\omega(T-t))$ and $g(T-t) = g(t)$ to get

$$\int_0^T y(g(t)) \begin{bmatrix} \cos(\omega t) \\ \sin(\omega t) \end{bmatrix} dt = 2 \int_0^{\frac{T}{2}} y(g(t)) \begin{bmatrix} \cos(\omega t) \\ 0 \end{bmatrix} dt. \quad (22)$$

Therefore, we conclude that the second component of the integral in (19) is zero. Using this and the definition of $\mathcal{U}$ in (19), we get

$$\gamma = \begin{bmatrix} \cos(\alpha) \\ \sin(\alpha) \end{bmatrix} \int_0^T y(g(t)) \cos(\omega t - \alpha) dt \quad (23)$$

If we introduce the change of variables $t' = t + t_0$ and take the norm of (23), we arrive at the expression (14a).

Finally, we show that the direction of $\gamma$ is the opposite direction of $c$ (which given by $[\cos(\alpha), \sin(\alpha)]^T$). To do so, we need only show that

$$\int_0^T y(g(t)) \cos(\omega t - \alpha) dt < 0. \quad (24)$$

If $\|c\| > 0$, we have

$$\int_0^T y(g(t)) \cos(\omega t - \alpha) dt = \int_0^{\frac{T}{2}} y(g(t)) \cos(\omega t - \alpha) dt + \int_{\frac{T}{2}}^T y(g(t)) \cos(\omega t - \alpha) dt. \quad (25)$$

Moreover, using the change of variables $t' = t - \pi/\omega$, in the integral that goes from $T/2$ to $T$ we get that (25) is equivalent to

$$\int_0^{\frac{T}{2}} \left( f(g(t)) - f\left( g\left( t + \frac{\pi}{\omega} \right) \right) \right) cos(\omega t - \alpha) dt \quad (26)$$

Recalling the fact that the function $y$ is strictly decreasing and inspecting (20), we get $g(t) < g\left(t + \frac{\pi}{\omega}\right)$. Thus (24) must be negative when $\|c\| > 0$. By inspection, we also have that if $||c|| = 0$, then $\|\gamma\| = 0$, which concludes the proof. ■

*Remark 1:* Prop. 1 shows that the agent does not need to know its global coordinate (which would require knowledge of the source location) for the SESC, since $\gamma$ can be computed using (11), which does not depend on the angle $\alpha$. Moreover, Prop. 1 also shows that the norm of $\gamma$ depends uniquely on $||c||$ and the direction of $\gamma$ is along that of $||c||$. This means the the SESC is invariant to rotation and we can always rotate the reference frame such that $c = \begin{bmatrix} ||c|| & 0 \end{bmatrix}^T$.

## III. Analysis of the SESC

In this section, we provide a method for formally analyzing the behavior of the SESC in the presence of disturbances. We begin by noting that we can pursue a discrete-time perspective since the goal is to drive the center location as close as possible to zero and, under the SESC, the center only updates at discrete time steps.

When the center position is updated, we must now take into account the fact that the source may also have moved. The discrete-time center update equation then becomes

$$c[k+1] = c[k] + k_p \gamma[k] + W[k], \quad (27)$$

where $W[k] = \int_{t_k}^{t_{k+1}} -w(t)dt$ and $t_k$ is the instant when the $k$-th revolution of the system starts. Note that $\|W[k]\|$ is bounded by $M_w T$. Similarly, $\gamma[k]$ can be rewritten as

$$\gamma[k] = \underbrace{\int_0^T f\left(\left\|c[k] + R\begin{bmatrix}\cos(\omega t)\\ \sin(\omega t)\end{bmatrix}\right\|\right)\begin{bmatrix}\cos(\omega t)\\ \sin(\omega t)\end{bmatrix} dt}_{\beta(c[k])} + V[k], \tag{28}$$

where $V[k]$ is effect of the disturbance $v(\cdot)$ in the measurements as well as effects due to source motion during the period $T$. In order to compute an upper bound on $\|V[k]\|$, we begin by computing the instantaneous relative position of the center with respect to the source during the $k$-th revolution:

$$s(t) = c[k] + R\begin{bmatrix}\cos(\omega t)\\ \sin(\omega t)\end{bmatrix} - \int_{t_k}^{t} w(t)dt. \tag{29}$$

Thus, $f(\|s(t) - x(t)\|)$ is given by

$$f\left(\left\|c[k] + R\begin{bmatrix}\cos(\omega t)\\ \sin(\omega t)\end{bmatrix}\right\|\right) + \tilde{v}(t), \tag{30}$$

where $\|\tilde{v}(t)\|$ is upper bounded by $f'_{\max} M_w (t - t_k)$ with $f'_{\max}$ being the maximum of the absolute value of the derivative of the function $f$. Thus,

$$\left\|\int_{t_k}^{t_{k+1}} \tilde{v}_k dt\right\| < \frac{T}{2} f'_{\max} K_w. \tag{31}$$

Additionally, since $\left\|\int_{t_k}^{t_{k+1}} v(t)dt\right\|$ is bounded by $K_v T$, we have that $\|V[k]\|$ is upper bounded by $T(f'_{\max} K_w/2 + K_v)$. Thus, the complete dynamics of the center of revolution can be described as

$$c[k+1] = c[k] + k_p \beta(c[k]) + k_p V[k] + W[k]. \tag{32}$$

The expression (32) has a surprisingly simple structure: $\beta[k]$ is a term that only depends on the value of $c[k]$ and the disturbances are additive and upper bounded. In the sequence, we develop a deeper understanding of $\beta(c[k])$, in order to use it to analyze the behavior of the system.

### A. Intepretation of $\beta(c[k])$

In (32), we see that $\beta(\cdot)$ is responsible for driving the revolution center towards the source. Note that from Prop. 1 the norm of $\beta(c[k])$ is invariant with respect to the orientation of the coordinate frame. Thus, the revolution center at time $k$ can be written as $c[k] = \begin{bmatrix}||c[k]|| & 0\end{bmatrix}^T$. From Prop. 1, we also know that $\beta(c[k])$ is in the opposite direction of $c[k]$. This means that, in the absence of disturbances, the SESC will move the revolution center directly towards the source.

In order to build intuition on the effectiveness of this restoring control, we numerically computed $||\beta(c[k])||$ as a function of the norm of $c[k]$ using

$$f(r) = \exp(r^2) \text{ and } f(r) = \frac{1}{(1+r)^2}, \tag{33}$$

and considered various values of $R$. The results are shown in Fig 1. From these plots, we see that the $||\beta(c[k])||$ has a unique peak and falls off rapidly as the distance to the source either decreases (the agent moves towards the source) or increases (the agent moves away from the source). Therefore, if the agent starts far from the source, any disturbance in the system may overwhelm the restoring force from $\beta$ and prevent convergence. Similarly, the disturbances will prevent perfect convergence to the source with the proximity defined by the shape of $\beta(\cdot)$ and the level of the disturbance.

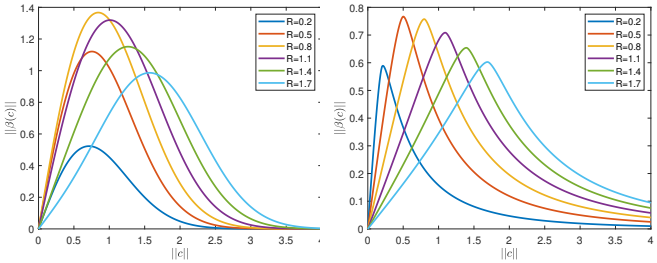


Fig. 1: Illustration of $\beta(c[k])$ as a function of $c[k]$ with (left) $f(r) = \exp(-r^2)$ and (right) $f(r) = \frac{1}{(1+r)^2}$.

With this intuition in hand, we now characterize the regions where the agent will be guaranteed to be pushed towards the source, even in the presence of disturbances and source movement. Towards this, we define the following set:

$$\mathcal{F} = \{c \in \mathbb{R}^2 \mid k_p||\beta(c)|| + D_{\max} < 2||c||, \quad k_p||\beta(c)|| > D_{\max}\} \tag{34}$$

where $D_{\max} = k_p T(f'_{\max} M_w/2 + M_v) + T M_w$ is the bound on the norm of the disturbance $W[k] + K_p V[k]$ in (32). This region $\mathcal{F}$ is illustrated in Fig. 2.

*Proposition 2:* If $c[k] \in \mathcal{F}$, then under the SESC, $||c[k+1]|| < ||c[k]||$.

*Proof:* As noted in (1), the SESC is invariant to rotation. Therefore, without loss of generality, we assume that $c[k] = \begin{bmatrix}x & 0\end{bmatrix}^T$ with $x > 0$ and that $\beta(c[k]) = \begin{bmatrix}-b & 0\end{bmatrix}^T$, for some $b > 0$. Thus, (32) gives that

$$c[k+1] = \begin{bmatrix}x - k_p b\\ 0\end{bmatrix} + k_p V[k] + W[k]. \tag{35}$$

Therefore, since $D_{\max}$ is an upper bound on $||K_p V[k] + W[k]||$, using the triangle inequality we have

$$||c[k+1]|| < |x - K_p b| + D_{\max}. \tag{36}$$

Since $c[k] \in \mathcal{F}$, we get

$$-(x - D_{\max}) < x - k_p b < x - D_{\max}. \tag{37}$$

Thus, $|x - K_p b| < x - D_{max}$. Using this in (36) yields

$$||c[k+1]|| < x = ||c[k]||. \tag{38}$$

■

*Remark 2:* Prop. 2 shows that for initial revolution center positions such that the agent is inside the region $\mathcal{F}$, the SESC guarantees to move the center towards the origin. Note that it does not establish asymptotic convergence to the origin, as the disturbance may overcome the restoring force when $||c|| < ||c||_{\min}$ (see Fig. 2). In the remainder of

the paper, when we refer to convergence, we mean that the revolution center approaches the set given by $||c|| \leq ||c||_{\min}$. Additionally, we note that the set $\mathcal{F}$ can be easily computed numerically since its computation consists in verifying the conditions in the definition of $\mathcal{F}$ and $||\beta(c)||$ is a function of a single variable ($||c||$) that can be efficiently computed using numerical integration (see Prop. 1).

By construction of the proof we see that the rate of convergence increases as $\|\beta(c[k])\|$ approaches $\|c[k]\|$. However, the converse is also true; that is, if $\|\beta(c[k])\|$ is on the order of the disturbance bound, then convergence can be very slow. This also highlights the fact that by computing the region $F$, we can predict the convergence of the controller, taking into account the disturbances. If the system begins outside these domains, then the disturbance may be larger than the ability of the SESC to move towards the source.

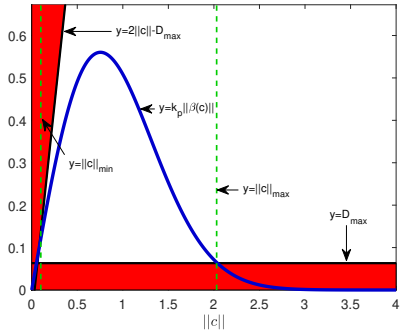


Fig. 2: Representation of $\mathcal{F}$. When $k_p||\beta(c)||$ (blue) is not in the red area (i.e. $\|c\|_{\min} < ||c|| < \|c\|_{\max}$), the rotation center will move towards the source. Here $f = \exp(-r^2), R = 0.5, T = 0.05, k_p = 0.5, M_w = 1, M_v = 0.1$.

## IV. Simulation and Experimental Results

In this section, we describe simulation and experimental results using both the SESC and the OESC in order to demonstrate the results and compare the predictions based on the SESC to the results using the OESC.

### A. Simulation Results

We first simulated the OESC and the SESC in order to compare their response. The parameters in (1)-(3) for both were set to $k_p = 0.5, R = 0.5, T = 0.01, M_w = 1, M_v = 0.1$. The disturbance and source movement were simulated using a random uniform noise, bounded according to $M_w$ and $M_v$. The scalar field was defined as $f(r) = \exp\left(-r^2\right)$. The values of $\beta$ for this specific setup are shown in Fig. 1.

The results of a simulation with an initial condition at $(2, 1.5)$ and run for 30 complete revolutions are shown in Fig. 3. This figure shows that the behavior of the two controllers is qualitatively similar. In the SESC, the agent makes a perfect circular orbit and then jumps to the next orbit as the center position updates. The OESC follows a smooth path (and is therefore physically implementable) with motions that are approximately circular with radius $R$. In both cases, the initial motion of the center position is

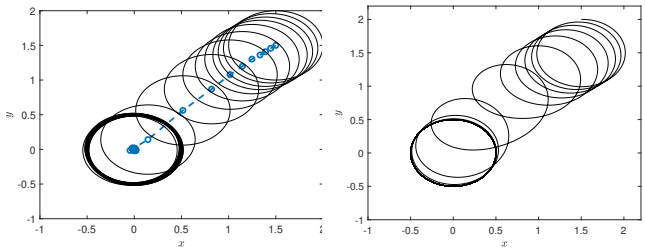

Fig. 3: Simulated trajectories using the SESC and OESC under equivalent conditions. (left) Agent trajectory (black) under the SESC and the revolution center (blue circle). (right) Agent trajectory (black) under the OESC.

slow; convergence then accelerates (most easily seen in the increasing distance between centers in Fig. 3) before slowing down again when the center gets close to the source at the origin. This, of course, reflects the shape of the restoring term defined by $\beta$ as shown in Fig. 1.

To investigate the region of attraction defined by the set $\mathcal{F}$, we performed a series of simulations with initial conditions selected such that the initial distance to the origin ranged from 0.1 to 4. For this particular choice of parameters, we have that $F = \{c \mid ||c||_{\min} < ||c|| < ||c_{\max}\}$ with $||c||_{min} = 0.07$ and and $||c_{\max}|| = 2.83$. We declared that a trajectory had converged when the rotation center had norm lower than $||c||_{\min}$, since if $||c|| < ||c||_{\min}$ we can not expect the rotation center to move closer to the source.

For each of these distances, we randomly chose 100 different initial locations and calculated the ratio of the number of runs that converged to the origin within 100 revolutions to the total number of runs. Based on Prop. 2, the expected maximum range of convergence for the parameters in these simulations was 2.83. The results of these simulations are shown in Fig. 4. In general, the SESC results match well with the prediction, though there are a small number of runs just prior to the boundary that did not achieve convergence. This was due to the fact that the convergence rate is small when starting right at the maximum distance, and depending on the realization of the disturbance in any particular run, 100 revolutions may not be sufficiently long. A more interesting result is that the prediction holds well for the OESC, though it is conservative. Since the OESC continuously updates its center location, it is more robust to disturbances and has a slightly higher chance to converge in practice than the SESC.

### B. Experimental Demonstration

We implemented the OESC using a direct-drive wheeled robot (iRobot Create 2) to demonstrate that the OESC is a practical controller, even in the face of practical realities, and to show that the phenomena predicted via the theoretical analysis of SESC (such as the existence of a radius of convergence based on the position of the center of revolution) are also observed in practice. Note that the SESC is not a practical controller as it demands instantaneous transitions between different circular orbits. Our results, then, only involve the OESC. All the code was implemented using ROS

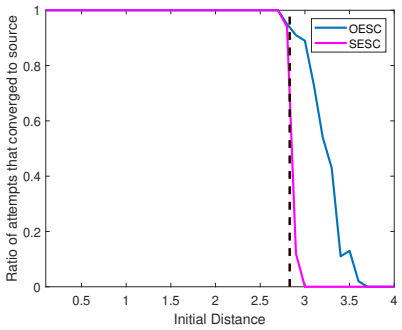


Fig. 4: Ratio of trajectories that converged after 100 full revolutions under the SESC (mauve) and the OESC (blue). (black dotted line) Maximum expected distance for convergence.

and Python 2.7 on a Raspberry Pi 2 running Ubuntu 18.04. The position of the agent was captured using a Optitrack motion capture system and these measurements, while of high quality, are subject to measurement noise. The source was created artificially, with movement using a simulated uniformly distributed disturbance with $M_w = 0.01$ m/s. The random signal was artificially generated according $f(r) = \exp(-2r^2)$, where $r$ is the distance in meters between the artificial source and the agent. To compute the bound on the measurement noise, $M_v$, we placed the robot at many fixed positions in the experimental area, measured the mean and the maximum deviation of the intensity calculated from the measured position and the form of $f(\cdot)$, and set $M_v$ to the maximum among these. For these experiments. we found $M_v = 0.03$ m.

The parameters of the OESC were set to $R = 0.54$ m, $T = 6.7$ s and $k_p = 0.2$. We computed the corresponding $\mathcal{F}$ and found that convergence of the revolution center towards the source was expected if $0.13 \text{ m} < \|c\| < 1.25$ m. We then ran experiments with two different initial conditions. The resulting trajectories and time traces of the rotation center are shown in Fig. 5 with an initial distance of 1.23 m (blue line) and 1.70 m (red line). As expected, at 1.23 m the robot converged to the a small region around the source while at 1.70 m it did not. To better illustrate the behavior of the robot after converging, we ran another experiment that focused on the region near the source; this trajectory is shown in Fig. 6.

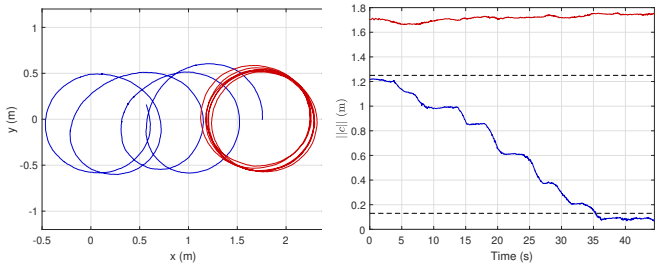


Fig. 5: OESC experimental results from initial conditions at a distance of (blue) 1.35 m and (red) 1.70 m from the source. (left) Robot trajectories. (right) Evolution of distance between revolution center and the source. (dotted black lines) Predicted bounds for convergence.

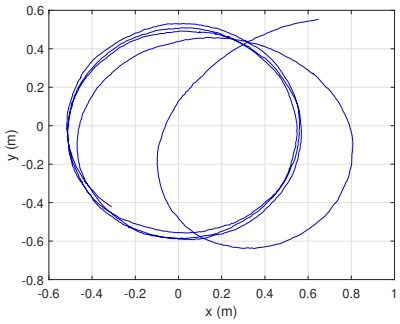


Fig. 6: OESC experimental trajectory, with special focus on the behavior after convergence.

These experimental results highlight one (perhaps) surprising result of our analysis, namely that it is not the position of the agent itself that matters but only its center of revolution. Observing the results in Fig. 5 we see that along the trajectory that failed to converge (red), the agent actually get closer to the source than the initial condition of the successful (blue) trajectory. However, the revolution center remained outside the region of convergence. The results also support the theoretical calculations of the region $\mathcal{F}$.

## V. CONCLUSION AND FUTURE WORK

In this work, we used a simplified version of a particular extremum seeking controller to develop intuition on its behavior in the presence of disturbances and analyzed its convergence properties. Through simulations we demonstrated that the analysis of the simplified version predicted the main aspects of the response of the original controller and effectively explained why convergence in the presence of disturbance is limited despite previous theoretical results showing global convergence. We were also able to provide insights on how the convergence speed of the controller vary with the distance between agent and source.

## REFERENCES

[1] S. C. Pinto, N. A. Vickers, F. Sharifi, and S. B. Andersson, "Tracking multiple diffusing particles using information optimal control," in *Proc. American Control Conference*, 2021, pp. 3935–3940.

[2] T. T. Ashley and S. B. Andersson, "Tracking a diffusing three-dimensional source via nonholonomic extremum seeking," *IEEE Transactions on Automatic Control*, vol. 63, no. 9, pp. 2855–2866, 2017.

[3] L. Calkins, R. Khodayi-mehr, W. Aquino, and M. M. Zavlanos, "Sensor planning for model-based acoustic source identification," in *Proc. American Control Conference*, 2020, pp. 2679–2684.

[4] P. Falcone, F. Colone, A. Macera, and P. Lombardo, "Localization and tracking of moving targets with wifi-based passive radar," in *Proc. IEEE Radar Conference*, 2012, pp. 0705–0709.

[5] Y. Tan, W. H. Moase, C. Manzie, D. Nešić, and I. M. Mareels, "Extremum seeking from 1922 to 2010," in *Proc. Chinese Control Conference*, 2010, pp. 14–26.

[6] S. Z. Khong, Y. Tan, C. Manzie, and D. Nešić, "Multi-agent source seeking via discrete-time extremum seeking control," *Automatica*, vol. 50, no. 9, pp. 2312–2320, 2014.

[7] M. Krstić and H.-H. Wang, "Stability of extremum seeking feedback for general nonlinear dynamic systems," *Automatica*, vol. 36, no. 4, pp. 595–601, 2000.

[8] D. Baronov and J. Baillieul, "A motion description language for robotic reconnaissance of unknown fields," *European Journal of Control*, vol. 17, no. 5-6, pp. 512–525, 2011.

[9] T. T. Ashley, E. L. Gan, J. Pan, and S. B. Andersson, "Tracking single fluorescent particles in three dimensions via extremum seeking," *Biomedical Optics Express*, vol. 7, no. 9, p. 3355, 2016.